COMMUNICATION

*S. Ahzi,*, A. Molinari,* and G. R. Canova**

# Effect of the Grain Shape on the Texture Evolution of a Polycrystalline Material

REFERENCE Ahzi, S., Molinari, A., and Canova, G. R., Effect of the grain shape on the texture evolution of a polycrystalline material, *Yielding, Damage, and Failure of Anisotropic Solids*, EGF5 (Edited by J. P. Boehler), 1990, Mechanical Engineering Publications, London, pp. 425–441.

ABSTRACT A viscoplastic self-consistent approach is formulated and used for texture modelling. At the single crystal level the viscoplasticity is modelled by non-linear viscous gliding on slip systems. For rolling and compression tests, the results of the self-consistent scheme are compared with experiments and with former homogenization schemes, i.e., the Taylor and relaxed Taylor theories. The improvements of the self-consistent approach rely on a better description of the interaction of a grain with the surroundings. The effects of grain shape are shown to be very important on the texture development. It is also shown that the self-consistent modelling tends to validate the relaxed Taylor assumption for large enough deformations.

## Introduction

The problem of the determination of the macroscopic constitutive behaviour of polycrystalline materials, from the microscopic elementary processes of deformation (micro–macro approach) is of considerable interest for practical purposes.

When large deformations are considered, the Taylor (1) and the relaxed Taylor theories (2), have been used extensively to derive the effective properties of aggregates.

Recently different self-consistent schemes have been proposed in the framework of large deformations, by Iwakuma and Nemat-Nasser (3), Lipinski and Berveiller (4) in time independent plasticity, and by Nemat-Nasser and Obata (5) and Molinari *et al.* (6) in viscoplasticity.

The model presented in (6) neglects elasticity since only applications for large deformations and quasi-proportional loading were considered. At the single crystal level the viscoplastic behaviour results from non-linear viscous gliding on the slip systems.

The self-consistent model was applied to texture simulations. It was shown to give some improvements with respect to former homogenization schemes, specially in the rolling and compression test. This was a result of the smaller

* Laboratoire de Mécanique et Physique des Matériaux, Faculté des Sciences, Ile de Saulcy, 57045 Metz Cedex 1, France.

interaction between a grain and the surrounding matrix, obtained in the self-consistent scheme.

Another definite improvement of the self-consistent approach relies on the possibility of taking account for the grain shapes (not the size) and of the interactions between grains in an $n$-site formulation. These effects are discussed here. Texture developments in rolling and compression are analysed and compared to the Taylor or relaxed Taylor theories.

The single crystal viscoplasticity is formulated in the following section, and the interaction laws between a grain and the surroundings are then discussed for the one-site self-consistent, as well as for the $n$-site self-consistent scheme. The localization problem, i.e., the calculation of the local strain rates and rotations from the macroscopic corresponding quantities, is then solved, and the shape effect is discussed in the subsequent section.

## Modelling

The viscoplastic behaviour of the single crystal is defined below. Elasticity is neglected since only applications for large deformations and quasi-monotonic paths of deformation are considered.

In order to calculate the effective properties of the aggregate, the localization problem (i.e., the calculation of the local stresses and strain rates) is solved with the aid of the interaction formula presented below.

### *Single crystal*

At the slip system level a flow law similar to a non-Newtonian viscous law (7)–(9) is considered

$$\tau^s/\tau_0^s = (\dot{\gamma}^s/\dot{\gamma}_o)^m \tag{1}$$

The shear rate $\dot{\gamma}^s$ of the slip system $s$ is related through a non-linear power law to the resolved stress

$$\tau^s = \mathbf{m}^s : \mathbf{S} = m_{ij}^s S_{ij} = b_i^s n_j^s S_{ij} \tag{2}$$

which is a projection on the slip direction $\mathbf{b}^s$ of the deviatoric stress vector acting on the slip plane of normal $\mathbf{n}^s$. The deviatoric Cauchy stress tensor is represented by $\mathbf{S}$. The second order tensor $\mathbf{m}^s$ is the tensorial product of the unit vectors $\mathbf{b}^s$ and $\mathbf{n}^s$. In the flow law, equation (1), $\dot{\gamma}_o$ is a reference strain rate, taken identical for each slip system, while $\tau_o^s$ is a reference stress evolving with the deformation (hardening).

This formulation, where all systems are active since there is no threshold in the flow law, equation (1), is interesting as it avoids the ambiguity problems appearing in the classical time independent formulation (9). Moreover, a

quasi-threshold is obtained when the strain rate sensitivity exponent $m$ tends to zero. Then the relation $\tau^s/\tau_o^s$ versus $\dot{\gamma}^s/\dot{\gamma}_o$, is almost a Heaviside step function, and $\tau_o^s$ is a quasi-threshold.

At the single crystal level, the flow law is a non-linear relation linking the strain rate tensor

$$D_{ij} = \frac{1}{2}\left(\frac{\partial v_i}{\partial x_j} + \frac{\partial v_j}{\partial x_i}\right) \tag{3}$$

(where the $v_i$ are the components of the velocity of particles and $x_i$ are cartesian coordinates in the laboratory frame) to the deviatoric stress S:

$$D_{ij}/\dot{\gamma}_o = \sum_s r_{ij}^s (r_{kl}^s S_{kl}/\tau_o^s)^n \tag{4}$$

with $n = 1/m$. This relation results from the combination of equations (1), (2), and the equation connecting **D** to the shear rate of all the slip systems

$$\mathbf{D} = \sum_s \mathbf{r}^s \dot{\gamma}^s \tag{5}$$

where $\mathbf{r}^s$ is the symmetrization of $\mathbf{m}^s$

$$\mathbf{r}^s = 1/2(\mathbf{m}^s + \mathbf{m}^{sT}) \tag{6}$$

From the flow law, equation (4), the hardening appears to rely upon two parts: the changes in $\tau_o^s$ represent the microscopic intracrystalline hardening, while the changes in the orientation factors $\mathbf{r}^s$ represent the texture (or geometrical) hardening.

It is usual to describe to first order, the intracrystalline hardening, by means of a linear relation between the rate of reference stresses and the microscopic shear rates

$$\dot{\tau}_o^s = \sum_r H^{sr}\dot{\gamma}^r \tag{7}$$

where $H^{sr}$ is the hardening matrix.

The geometrical hardening is related to the lattice rotation which is governed by the tensor of rate of lattice rotation $\mathbf{\Omega}^*$ defined, for example, in (9). It is linked to the total rate of rotation $\mathbf{\Omega}$ and the rate of plastic rotation $\mathbf{\Omega}^p$ by:

$$\mathbf{\Omega} = \mathbf{\Omega}^* + \mathbf{\Omega}^p \tag{8}$$

Since elasticity is neglected in this paper, the lattice is not distorted, and $\mathbf{\Omega}^*$ results solely from a rigid grain rotation. The tensor $\mathbf{\Omega}$ is the antisymmetric part of the velocity gradient $\mathbf{L} = \partial \mathbf{v}/\partial \mathbf{x}$.

$$\mathbf{\Omega} = 1/2(\mathbf{L} - \mathbf{L}^T) \tag{9}$$

while $\Omega^p$ is related to the microscopic shear rates

$$\Omega^p = \sum_s 1/2(\mathbf{m}^s - \mathbf{m}^{sT})\dot{\gamma}^s \tag{10}$$

Therefore $\Omega^*$ can be calculated when $\Omega$ and the $\dot{\gamma}^s$ are known.

One of the most interesting points in the present viscoplastic formulation results from the possibility of inverting the constitutive law (4). That law expressing D versus S can be written

$$D_{ij} = \mathcal{D}_{ij}(\mathbf{S}) \tag{11}$$

The inversion of (11), i.e., the calculation of S versus D

$$S_{kl} = \mathcal{S}_{kl}(\mathbf{D}) \tag{12}$$

is possible since there exists a convex viscoplastic potential.

*Interaction formula*

Likewise, at the level of the polycrystalline material, the macroscopic deviatoric stress $\bar{\mathbf{S}}$ is a non-linear function of the macroscopic strain rate $\bar{\mathbf{D}}$

$$\bar{\mathbf{S}} = \bar{\mathcal{S}}(\bar{\mathbf{D}})$$

The function $\bar{\mathcal{S}}$ characterizes the unknown effective behaviour of the polycrystalline material. Assuming that the macroscopic velocity gradient $\bar{\mathbf{L}} = \partial\bar{\mathbf{v}}/\partial\mathbf{x}$ is given ($\bar{\mathbf{v}}$ is the macroscopic velocity field), the goal is to calculate the local strain rate D and rotation $\Omega$ (localization process). Then the effective properties follow easily (homogenization process).

In Molinari *et al.* (6), an interaction formula is obtained which is useful for the localization calculation. From the equilibrium equations and the incompressibility condition, integral equations are obtained, in terms of the unknown strain rate D and the rate of rotation $\Omega$. Under the assumption of uniformity of D and $\Omega$ in each grain, these integral equations are discretized, leading to a non-linear system of algebraic equations where the unknowns are the strain rates $\mathbf{D}^g$ and the rate of rotation $\Omega^g$ in each grain $g$, as well as the effective properties of the Homogeneous Equivalent Medium (HEM).

To simplify the resolution of these equations, two approximate self-consistent schemes can be used. In the one-site self-consistent scheme, each grain is considered as an inclusion surrounded by the HEM. Then, assuming that the HEM can be represented by its tangent behaviour at $\bar{\mathbf{D}}$ (first order Taylor expansion at $\bar{\mathbf{D}}$), the one-site interaction formula is derived (6)

$$\mathbf{S}^g - \bar{\mathbf{S}} = \{(\Gamma^{gg})^{-1} + \mathbf{A}^\circ\} : (\mathbf{D}^g - \bar{\mathbf{D}}) \tag{14}$$

where the : represents a double contracted product.

In this relation the deviation between the macroscopic stress $\bar{\mathbf{S}}$ and the stress $\mathbf{S}^g$ in the grain $g$ is linked to the deviation between the macroscopic strain rate $\bar{\mathbf{D}}$ and the local $\mathbf{D}^g$. The macroscopic properties are explicitly represented by the effective tangent modulus at $\bar{\mathbf{D}}$

$$A^{\circ}_{klmn}(\bar{\mathbf{D}}) = \partial \bar{\mathcal{S}}_{kl}/\partial \bar{D}_{mn}(\bar{\mathbf{D}}) \tag{15}$$

The local behaviour is implicitly present since $\mathbf{S}^g$ and $\mathbf{D}^g$ are linked by the local constitutive law (4).

Finally, the grain morphology is included in the fourth order tensor $\Gamma^{gg}$ defined by

$$\Gamma^{gg} = \frac{1}{V_g}\int_{V_g}\left\{\int_{V_g}\Gamma(\mathbf{r}-\mathbf{r}')\,\mathrm{d}^3r'\right\}\mathrm{d}r^3 \tag{16}$$

where $V_g$ is the volume of the grain. The components of the tensor $\Gamma$ are defined in terms of the Green functions $G_{ni}$ depending solely on the effective modulus $\mathbf{A}^{\circ}$ (6)

$$\Gamma_{ijmn} = \tfrac{1}{4}(G_{im,jn} + G_{jm,in} + G_{in,jm} + G_{jn,im}) \tag{17}$$

The notation $(\Gamma^{gg})^{-1}$ in (14) is employed for the inverse of the tensor $\Gamma^{gg}$.

The way to calculate $\Gamma^{gg}$ for an ellipsoïdal grain is summarized in Appendix 1. In the general case the calculation is performed numerically. For the special case of a spherical grain and an isotropic tensor $\mathbf{A}^{\circ}$, simple analytical results for $\Gamma^{gg}$ are available.

The interaction formula (14) will be used to calculate the local stress and strain rates $\mathbf{S}^g$ and $\mathbf{D}^g$. When these quantities are known, the local rate of rotation $\Omega^g$ is obtained using the one-site interaction formula (6)

$$\Omega^g - \bar{\Omega} = \mathbf{B}^{gg} : (\Gamma^{gg})^{-1} : (\mathbf{D}^g - \bar{\mathbf{D}}) \tag{18}$$

where

$$\mathbf{B}^{gg} = \frac{1}{V_g}\int_{V_g}\left\{\int_{V_g}\mathbf{B}(\mathbf{r}-\mathbf{r}')\,\mathrm{d}\mathbf{r}'^3\right\}\mathrm{d}r^3 \tag{19}$$

The components of the tensor $\mathbf{B}$, given by

$$B_{ijmn} = \tfrac{1}{4}(G_{im,jn} - G_{jm,in} + G_{in,jm} - G_{jn,im}) \tag{20}$$

are calculated in Appendix 1.

It is emphasized that the one-site approach relies upon three main assumptions.

(1) The uniformity of strain rates in each grain.
(2) The localization problem is solved by considering a grain as an inclusion embedded in the HEM.
(3) The behaviour of the HEM is approximated by its tangent behaviour at $\bar{\mathbf{D}}$.

Actually it is well known that intragranular strain rate non-uniformities appear, especially at large deformations, but information about these inhomogeneities is still insufficient to be taken into account here.

The drawbacks which proceed from the second hypothesis can be reduced by considering an $n$-site formulation. Then the inclusion problem is solved for a grain $g$ embedded in an aggregate constituted by its $(n-1)$ nearest neighbours, the aggregate being itself embedded in the HEM (**6**)(**10**). Thus the interaction of a grain with its surroundings is accounted for in a better way. Hypothesis (3) above is still used for the HEM, but the approximations linked to hypothesis (3) are viewed to have less effects in the $n$-site self-consistent scheme.

The one-site scheme can be reasonably used for materials with no large heterogeneities. Indeed, the approximation of the matrix behaviour by a first-order Taylor expansion at $\bar{\mathbf{D}}$ is reasonable when the deviations of the strain rate $\mathbf{D}$ from $\bar{\mathbf{D}}$ are not too large. For materials presenting pronounced heterogeneities (e.g., strong anisotropies in hexagonal materials, two phase materials, etc.) the use of the $n$-site scheme is recommended.

Let us call $E_g$ the set of neighbouring grains $g'$ of the grain $g$. From results presented in Molinari *et al.* (**6**), the following interaction formulas are obtained

$$\mathbf{S}^g - \bar{\mathbf{S}} = \{(\boldsymbol{\Gamma}^{gg})^{-1} + \mathbf{A}^\circ\} : (\mathbf{D}^g - \bar{\mathbf{D}}) - (\boldsymbol{\Gamma}^{gg})^{-1} : \sum_{\substack{g' \in E_g \\ g' \neq g}} \boldsymbol{\Gamma}^{gg'} : \{\mathbf{S}^{g'} - \bar{\mathbf{S}} + \mathbf{A}^\circ : (\bar{\mathbf{D}} - \mathbf{D}^{g'})\} \tag{21}$$

$$\boldsymbol{\Omega}^g - \bar{\boldsymbol{\Omega}} = \mathbf{B}^{gg} : (\boldsymbol{\Gamma}^{gg})^{-1} : [\mathbf{D}^g - \bar{\mathbf{D}}) + \sum_{\substack{g' \in E_g \\ g' \neq g}} \{\mathbf{B}^{gg'} - \mathbf{B}^{gg} : (\boldsymbol{\Gamma}^{gg})^{-1} : \boldsymbol{\Gamma}^{gg'}\} : \{\mathbf{S}^{g'} - \bar{\mathbf{S}} + \mathbf{A}^\circ : (\bar{\mathbf{D}} - \mathbf{D}^{g'})\} \tag{22}$$

If $E_g$ is reduced to the grain $g$, the former one-site scheme is obtained. Then formulas (21) and (22) are reduced to (14) and (18). In the interaction formulas (21) and (22) the coupling between the grain $g$ and grains $g'$ is accounted for. The influence tensors $\boldsymbol{\Gamma}^{gg'}$ and $\mathbf{B}^{gg'}$ are defined by

$$\boldsymbol{\Gamma}^{gg'} = \frac{1}{V_g} \int_{V_g} \left\{ \iint_{V_{g'}} \boldsymbol{\Gamma}(\mathbf{r} - \mathbf{r}') \, \mathrm{d}r'^3 \right\} \mathrm{d}r^3 \tag{23}$$

$$\mathbf{B}^{gg'} = \frac{1}{V_g} \int_{V_g} \left\{ \iint_{V_{g'}} \mathbf{B}(\mathbf{r} - \mathbf{r}') \, \mathrm{d}r'^3 \right\} \mathrm{d}r^3 \tag{24}$$

The $n$-site self-consistent scheme is considered to take a better account of the interactions between neighbouring grains.

EF

*Scheme of calculation*

In order to solve the lo
the tangent modulus o

$$\mathbf{A}^\circ = 2\mu^* \mathbf{I}$$

where $\mathbf{I}$ is the fourth o

$$\mathbf{I}_{ijkl} = \tfrac{1}{2}(\delta_{ik}\delta_{jl} + \delta_{il}\delta$$

There is no obstacle t
calculations, somewha

The scheme of cal
gradient $\bar{\mathbf{L}}$ is given. Th
of $\bar{\mathbf{L}}$) and the rate of ro
microhardening param
given. We have to calcu
stresses $\mathbf{D}$, $\mathbf{S}$, the local

In the framework of
(14) and the single crys
rate and the stress in c

$$\mathbf{D}^g = \mathbf{D}^g(\mu^*, \bar{\mathbf{S}})$$

$$\mathbf{S}^g = \mathbf{S}^g(\mu^*, \bar{\mathbf{S}})$$

Then the relations

$$\bar{\mathbf{D}} = \langle \mathbf{D} \rangle$$

$$\bar{\mathbf{S}} : \bar{\mathbf{D}} = \langle \mathbf{S} : \mathbf{D} \rangle$$

between the macrosco
corresponding volumic
$\mathbf{D}^g$, $\mathbf{S}^g$, and the $\dot{\gamma}^s$ follow
of plastic rotation $\boldsymbol{\Omega}^{pg}$
rate of rotation $\boldsymbol{\Omega}^g$. Th

At time $t + \Delta t$, the $\tau_o^s$
$\boldsymbol{\Omega}^{*g}$ and the shapes c
gradient

$$\mathbf{L}^g = \mathbf{D}^g + \boldsymbol{\Omega}^g$$

For the $n$-site self-
consider a cubic repres
by periodicity. For e
volume, we consider
formula (21). This, a
results in a set of $2M$ c

*Scheme of calculation*

In order to solve the localization problem in a simple way, we assume here that the tangent modulus of the HEM is isotropic

$$\mathbf{A}^{\circ} = 2\mu^{*}\mathbf{I} \tag{25}$$

where $\mathbf{I}$ is the fourth order identity tensor on symmetric tensors defined by

$$\mathbf{I}_{ijkl} = \tfrac{1}{2}(\delta_{ik}\,\delta_{jl} + \delta_{il}\,\delta_{jk}) \tag{26}$$

There is no obstacle to solving the general case where $\mathbf{A}^{\circ}$ is anisotropic; the calculations, somewhat longer, are presented elsewhere.

The scheme of calculation is the following. The macroscopic velocity gradient $\bar{\mathbf{L}}$ is given. Therefore the macroscopic strain rates $\bar{\mathbf{D}}$ (symmetric part of $\bar{\mathbf{L}}$) and the rate of rotation $\bar{\mathbf{\Omega}}$ (antisymmetric part) are known. At time $t$, the microhardening parameters $\tau_{o}^{s}$, the orientations and the shapes of all grains are given. We have to calculate the effective modulus $\mu^{*}$, the local strain rates and stresses $\mathbf{D}$, $\mathbf{S}$, the local lattice rotation $\mathbf{\Omega}^{*}$, and the shear rates $\dot{\gamma}^{s}$ in each grain.

In the framework of the one-site self-consistent scheme, the interaction law (14) and the single crystal constitutive law (4) are used to calculate the strain rate and the stress in each grain $g$ as a function of $\mu^{*}$ and $\bar{\mathbf{S}}$

$$\mathbf{D}^{g} = \mathbf{D}^{g}(\mu^{*}, \bar{\mathbf{S}}) \tag{27}$$

$$\mathbf{S}^{g} = \mathbf{S}^{g}(\mu^{*}, \bar{\mathbf{S}}) \tag{28}$$

Then the relations

$$\bar{\mathbf{D}} = \langle \mathbf{D} \rangle \tag{29}$$

$$\bar{\mathbf{S}} : \bar{\mathbf{D}} = \langle \mathbf{S} : \mathbf{D} \rangle \tag{30}$$

between the macroscopic strain rate (respective rate of plastic work) and the corresponding volumic average, are used to calculate $\mu^{*}$ and $\bar{\mathbf{S}}$. The values of $\mathbf{D}^{g}$, $\mathbf{S}^{g}$, and the $\dot{\gamma}^{s}$ follow immediately from (27), (28) and (1), (2). The local rate of plastic rotation $\mathbf{\Omega}^{pg}$ is given by (10). The interaction law (18) gives the total rate of rotation $\mathbf{\Omega}^{g}$. The lattice rotation $\mathbf{\Omega}^{*g}$ follows from (8).

At time $t + \Delta t$, the $\tau_{o}^{s}$ are updated with (7). The new orientations follow from $\mathbf{\Omega}^{*g}$ and the shapes of the grains are updated knowing the local velocity gradient

$$\mathbf{L}^{g} = \mathbf{D}^{g} + \mathbf{\Omega}^{g}$$

For the $n$-site self-consistent scheme, the procedure is similar. Let us consider a cubic representative volume of $M$ grains. This volume is reproduced by periodicity. For each grain among the $M$ grains in the representative volume, we consider a cluster of $n$ grains and apply the $n$-site interaction formula (21). This, added to the constitutive law (4) of each single crystal, results in a set of $2M$ coupled tensorial equations. The $2M$ tensorial unknowns

$\mathbf{D}^g$ and $\mathbf{S}^g$ can be obtained as functions of $\mu^*$ and $\bar{\mathbf{S}}$. These last quantities are calculated in order to fulfil the conditions (29) and (30).

## Results

Applications to the calculation of texture development are considered for rolling and compression tests. The influence of the grain shape is discussed here. The effects of the interactions between grains will be presented in a forthcoming paper.

A polycrystalline FCC material is considered with 100 grains having initial random orientations. The initial texture is therefore isotropic. We assume an isotropic linear hardening of the slip systems, as in OFHC copper. Thus the hardening law for the reference stresses $\tau_o^s$ takes the following form

$$\frac{\dot{\tau}_o^s}{\tau_o^o} = 0.1\dot{\Gamma} \tag{31}$$

where $\tau_o^o$ is the initial reference stress, identical for each slip system, and

$$\dot{\Gamma} = \sum_s |\dot{\gamma}^s| \tag{32}$$

The microscopic strain rate sensitivity is taken to be

$$m = 0.02 \tag{33}$$

The macroscopic equivalent plastic strain rate $\bar{D}_{eq}$ and plastic strain $\bar{\varepsilon}_{eq}$ are defined by

$$\bar{D}_{eq} = \sqrt{(\tfrac{2}{3}\bar{D}_{ij}\bar{D}_{ij})} \quad \bar{\varepsilon}_{eq} = \int_0^t \bar{D}_{eq}(\tau)\, d\tau \tag{34}$$

In (6), the proposed viscoplastic self-consistent model was used to predict texture development in different mechanical tests – tension, compression, rolling, torsion – with good agreement with respect to experimental results. The deformations were no larger than $\bar{\varepsilon}_{eq} = 1$, and the modifications in the shape of the grains were neglected. Here, the shape effect is accounted for, and deformations up to $\bar{\varepsilon}_{eq} = 2$ will be explored in the framework of the one-site self-consistent scheme. The initial shape of grains is assumed spherical. It appears that the evolution from the spherical shape to an elongated ellipsoïd for large deformations, plays a definite role in the final texture. Two tests are considered, rolling and compression.

### *Rolling*

For the rolling test, the non-zero components of the imposed macroscopic velocity gradient are



$$\bar{L}_{11} = \dot{\gamma}_o \quad \bar{L}_{33} = -\dot{\gamma}_o$$

Figures 1–3 represent
mation. For $0 \leq \bar{\varepsilon}_{eq} \leq 0$
observed, Fig. 1. One ca
intensity in the rolling di
component which is ob
where the strain rates are
copper component. The
cal arguments, would pr
not relevant here, sinc
deformation.

The better results obt
the lower interaction b
theory, as discussed in (
The fact that the sha
$\bar{\varepsilon}_{eq} = 0.5$, where the sha
results are almost identi
For $\bar{\varepsilon}_{eq} \geq 1$, the shape
$S$ components are devel
If the shape is not u
almost a fibre-type textu
For $\bar{\varepsilon}_{eq} > 1.5$, the calc
components $D_{11}$, $D_{22}$,
quantities. Therefore, f
relaxed Taylor theory,
heuristic arguments bas
The mixture of copp
observed in experiment

### *Compression*

A compression test is
imposed

$$\bar{L}_{11} = \bar{L}_{22} = \tfrac{1}{2}\dot{\gamma}_o$$
$$\bar{L}_{33} = -\dot{\gamma}_o$$

The other components
figures representing the
(for each grain). It app
tration of the orientati
neither by the Taylor n
The grain shape effe
Fig. 5, where the meas

$$\bar{L}_{11} = \dot{\gamma}_o \quad \bar{L}_{33} = -\dot{\gamma}_o \tag{35}$$

Figures 1–3 represent (111) pole figures at different stages of the deformation. For $0 \leq \bar{\varepsilon}_{eq} \leq 0.5$, the development of a copper-type texture can be observed, Fig. 1. One can observe specially that the (111) poles have a peak of intensity in the rolling direction axis. This corresponds to the so-called copper component which is observed in experiments. The classical Taylor model, where the strain rates are assumed uniform in the aggregate, cannot predict this copper component. The relaxed Taylor theory, which is based on morphological arguments, would predict the correct copper component, but this theory is not relevant here, since the change of shape is small at these stages of deformation.

The better results obtained here with the self-consistent scheme, are due to the lower interaction between the grain and the matrix than in the Taylor theory, as discussed in (6).

The fact that the shape effect is small here, is illustrated in Fig. 1(b) for $\bar{\varepsilon}_{eq} = 0.5$, where the shape has not been updated. Compared with Fig. 1(a), the results are almost identical.

For $\bar{\varepsilon}_{eq} \geq 1$, the shape effect will be significant. In Fig. 2 it appears that some $S$ components are developing as well as a little brass component.

If the shape is not updated, the texture at $\bar{\varepsilon}_{eq} = 2$ is quite different: it is almost a fibre-type texture, Fig. 3.

For $\bar{\varepsilon}_{eq} > 1.5$, the calculations indicate that the local values of the strain rate components $D_{11}$, $D_{22}$, $D_{33}$, $D_{12}$ tend to the corresponding macroscopic quantities. Therefore, for large deformations, we obtain a coincidence with the relaxed Taylor theory, which assumes these constraints by considering some heuristic arguments based on the morphology of the grains.

The mixture of copper, $S$, and brass components appearing in Fig. 2(b) is observed in experimental results, Bacroix (11).

*Compression*

A compression test is considered now. The following velocity gradient is imposed

$$\bar{L}_{11} = \bar{L}_{22} = \tfrac{1}{2}\dot{\gamma}_o \qquad \bar{L}_{33} = -\dot{\gamma}_o \tag{36}$$

The other components are equal to zero. Figures 4(a) and 4(b) are inverse pole figures representing the orientation of the compression axis in the crystal axis (for each grain). It appears (Fig. 4(a)) that for $\bar{\varepsilon}_{eq} = 0.75$, there is a concentration of the orientations in the vicinity of the (011) axis. This is predicted neither by the Taylor nor by the relaxed Taylor theory.

The grain shape effects expected for higher deformations are illustrated in Fig. 5, where the measures $\delta_i$ of the deviation of the strain rates between the

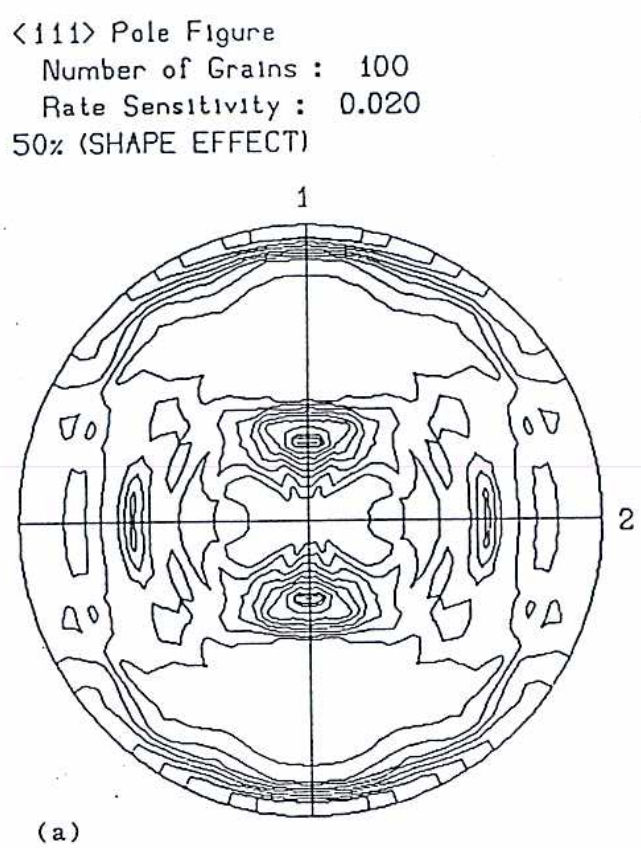


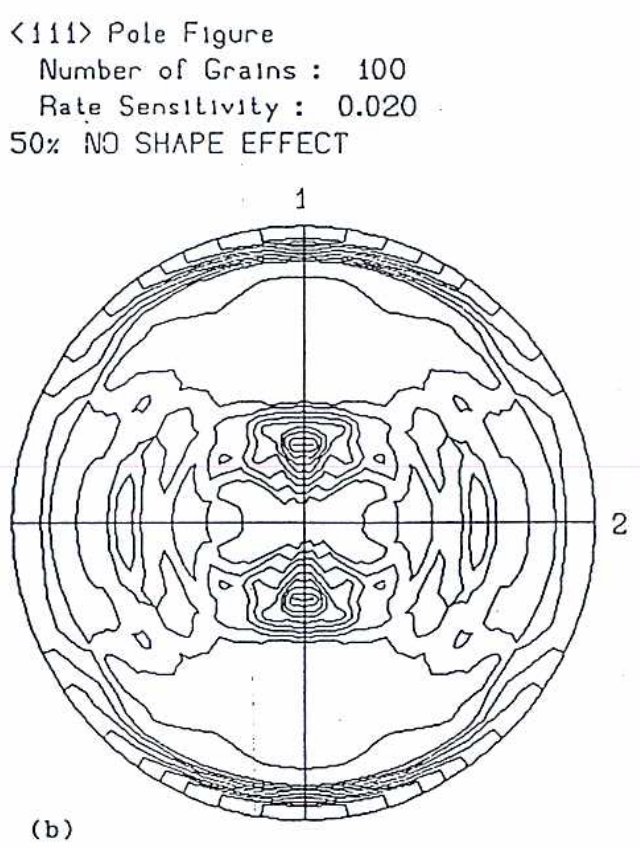


**Fig 1** These (111) pole figures represent the copper-type texture obtained for a macroscopic equivalent von Mises deformation $\bar{\varepsilon}_{eq} = 0.5$ in a rolling test. The initial grain shape is spherical. The shape is updated in Fig. 1(a) and not updated in Fig. 1(b). The textures are almost identical, showing that the change of shape has little effect for this small deformation

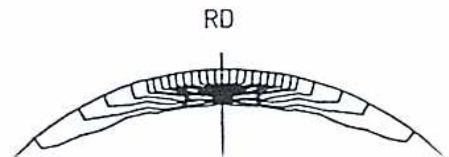


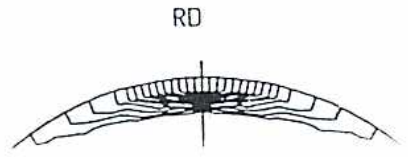

(a) (b)

Fig 1 These (111) pole figures represent the copper-type texture obtained for a macroscopic equivalent von Mises deformation $\bar{\varepsilon}_{eq} = 0.5$ in a rolling test. The initial grain shape is spherical. The shape is updated in Fig. 1(a) and not updated in Fig. 1(b). The textures are almost identical, showing that the change of shape has little effect for this small deformation



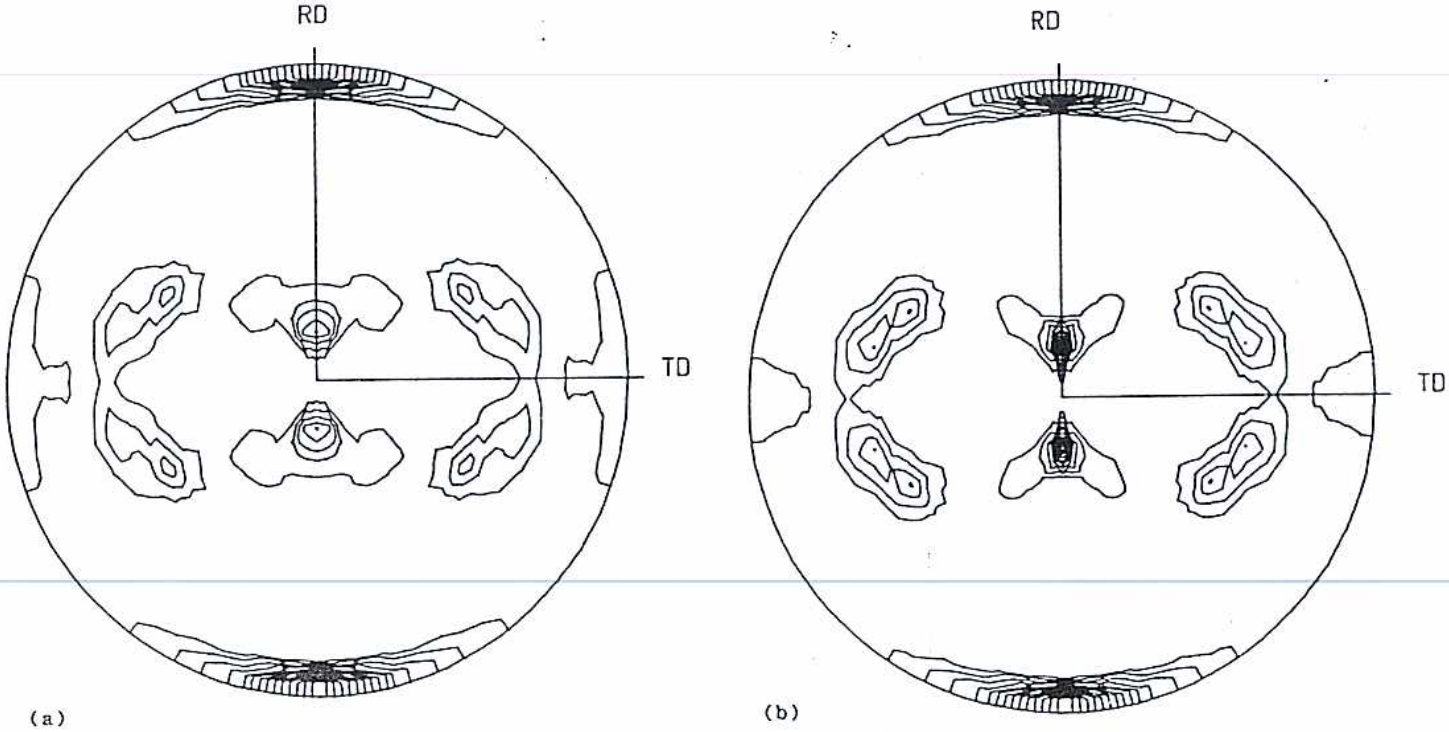


(a) (b)

Fig 2 Development of $S$ components in the copper type texture, for (a) $\bar{\varepsilon}_{eq} = 1.5$, and (b) $\bar{\varepsilon}_{eq} = 2$. A little brass component is also appearing. The shape is updated

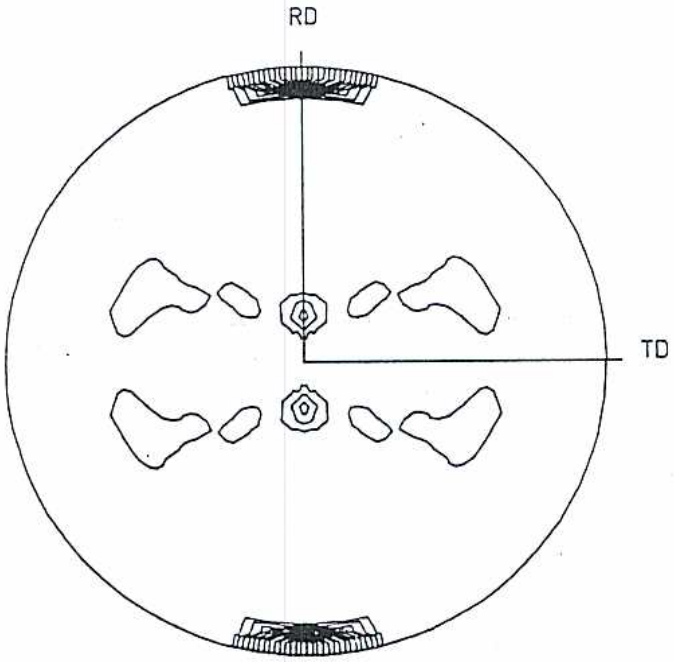


Fig 3 The shape is not updated. At $\bar{\varepsilon}_{eq} = 2$, a fibre-type texture is obtained

grains and the matrix are represented as a function of the equivalent macroscopic von Mises deformation, $\bar{\varepsilon}_{eq}$. The following strain rate vector is defined, Lequeu *et al.* (12)

$$\begin{aligned} D_1 &= (D_{22} - D_{11})/\sqrt{2} \\ D_2 &= \sqrt{3/2}\, D_{33} \\ D_3 &= \sqrt{2}\, D_{23} \\ D_4 &= \sqrt{2}\, D_{13} \\ D_5 &= \sqrt{2}\, D_{12} \end{aligned} \tag{37}$$

The standard deviation between the local strain rate $D_i$ and the macroscopic strain rate $\bar{D}_i$, is defined by

$$\delta_i = \frac{1}{N} \sum_{g=1}^{N} (\bar{D}_i - D_i^g)^2 \tag{38}$$

where the summation holds on all the grains.

For $\bar{\varepsilon}_{eq}$ large enough (i.e., $\geqslant 1$) $\delta_1$, $\delta_2$, and $\delta_5$ tend to zero, Fig. 5. This means that $D_{11}$, $D_{22}$, $D_{33}$, $D_{12}$ are constrained to take the macroscopic values $\bar{D}_{11}$, $\bar{D}_{22}$, $\bar{D}_{33}$, $\bar{D}_{12}$ as in the relaxed Taylor theory. Due to this transition to the

Fig 4 These inverse pole figures represent the texture in a compression test.
(a) For $\bar{\varepsilon}_{eq} = 0.75$ a concentration of the orientations in the vicinity of the (011) axis is observed. The grain shapes have little influence.
(b) For $\bar{\varepsilon}_{eq} = 1.5$, the shape effects are leading to a transition to the relaxed Taylor theory. The (011) relative intensity is decreasing

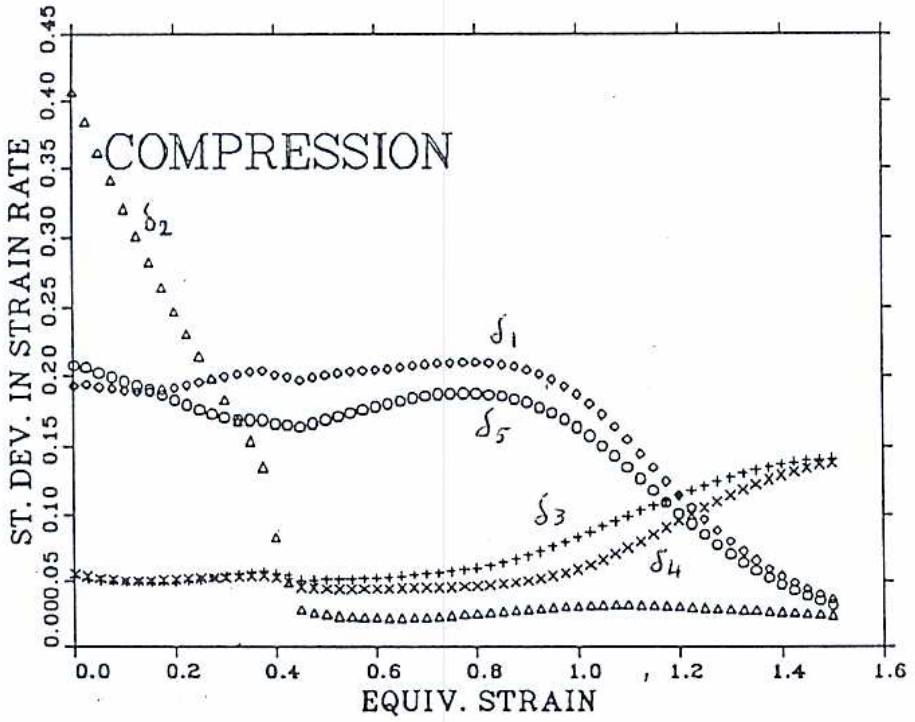


Fig 5 Evolution versus $\bar{\varepsilon}_{eq}$ of the standard deviations $\delta_i$ between the strain rate in the grains and the macroscopic strain rate. For $\bar{\varepsilon}_{eq} \geq 1$, $\delta_1$, $\delta_2$, and $\delta_5$ are tending to zero. This is a manifestation of strong morphological effects leading to a transition to the relaxed Taylor theory

relaxed Taylor theory, some orientations are leaving the (011) axis, for $\bar{\varepsilon}_{eq} = 1.5$, Fig. 4(b), decreasing the (011) relative intensity. The type of texture represented in Fig. 4(b) has been observed by Hansen and Leffers in the case of copper (13).

## Conclusion

The improvement of this viscoplastic self-consistent approach with respect to the Taylor theory (fully or relaxed constrained, respectively FC or RC) relies upon the following.

(1) The lower interaction between the grain and the surroundings in the self-consistent approach, even in the absence of strong morphological anisotropy.
(2) The possibility of including, in a continuous way, the evolution of the grain shape, and therefore taking account of morphological texture.

(3) The possibility
grains.

The lower interacti
FC or RC theories i
(as in RC Taylor) wc
FC and RC Taylor
orientations near (01

The grain morpho
evolution. To discuss
(spherical grains). A
phology leads to a tr
accounting for the gr
which are in better a
texture at large defor

## Appendix 1

*Calculation of the ten*

The calculation of th
the elastic problem tr
here by the tangent n
also (6) Appendix C)

$$\Gamma^{gg}_{ijmn} = 1/4(P^{gg}_{ijmn} +$$

$$B^{gg}_{ijmn} = 1/4(P^{gg}_{ijmn} -$$

where the $P_{ijmn}$ are d

$$P^{gg}_{ijmn} = \frac{1}{V_g}\int_{V_g}\left\{\int_{V_g}$$

These quantities are

$$P^{gg}_{ijmn} = -\frac{1}{4\pi}\int_0^{\pi} \sin$$

where the Fourier tra
following system

$$-A^{\circ}_{ijkl}k_l k_j \tilde{G}_{km}(\mathbf{k}) +$$

The Green functions
(6).

In (42), spherical
matrix $\psi$ is defined b

(3) The possibility of describing, in some way, the interactions between grains.

The lower interaction (1) has been shown (6) to lead to better results than the FC or RC theories in rolling and compression. No morphological arguments (as in RC Taylor) were necessary to predict the copper component in rolling. FC and RC Taylor theories were unable to predict the concentration of orientations near (011) in compression.

The grain morphology is shown to have a definite effect on the texture evolution. To discuss this effect, an initial isotropic morphology was assumed (spherical grains). At large deformations, the strong anisotropy of the morphology leads to a transition to the RC Taylor theory. The continuous way of accounting for the grain shape in the calculations, leads to texture predictions which are in better agreement with experimental results (e.g., in rolling, the texture at large deformations is a mixture of copper, $S$, and brass components).

## Appendix 1

*Calculation of the tensors $\Gamma^{gg}$ and $B^{gg}$ for an ellipsoïdal inclusion*

The calculation of the coefficients $\Gamma^{gg}_{ijmn}$ and $B^{gg}_{ijmn}$ follows the same lines as in the elastic problem treated by Tiem *et al.* (14). The elastic tensor $c^o$ is replaced here by the tangent modulus $A_o$. The main results are summarized here (see also (6) Appendix C). From (16), (17) and (19), (20) it follows that

$$\Gamma^{gg}_{ijmn} = 1/4(P^{gg}_{ijmn} + P^{gg}_{jimn} + P^{gg}_{ijnm} + P^{gg}_{jinm}) \tag{39}$$

$$B^{gg}_{ijmn} = 1/4(P^{gg}_{ijmn} - P^{gg}_{jimn} + P^{gg}_{ijnm} - P^{gg}_{jinm}) \tag{40}$$

where the $P_{ijmn}$ are defined by integrals over the volume $V_g$ of the inclusion

$$P^{gg}_{ijmn} = \frac{1}{V_g}\int_{V_g}\left\{\iint_{V_g} G_{im,jn}(\mathbf{r}-\mathbf{r}')\,dr'^3\right\}dr^3 \tag{41}$$

These quantities are given by

$$P^{gg}_{ijmn} = -\frac{1}{4\pi}\int_0^{\pi}\sin\theta\left\{\int_0^{2\pi}\psi_{jr}k_r\psi_{ns}k_s\tilde{G}_{im}(\psi\mathbf{k})\,d\Phi\right\}d\theta \tag{42}$$

where the Fourier transform $\tilde{G}_{im}(\mathbf{k})$ of the Green functions are solutions of the following system

$$\begin{aligned} -A^{o}_{ijkl}k_jk_j\tilde{G}_{km}(\mathbf{k}) + e^{i\pi/2}k_i\tilde{H}_m(\mathbf{k}) + \delta_{im} &= 0 \\ k_k\tilde{G}_{km}(\mathbf{k}) &= 0 \end{aligned} \tag{43}$$

The Green functions $H_m$ are linked to the hydrostatic pressure, Molinari *et al.* (6).

In (42), spherical coordinates of $\mathbf{k}$ are used, $k$, $\theta$, $\Phi$ with $k_3 = k\cos\theta$. The matrix $\psi$ is defined by

$$\psi = \begin{bmatrix} 1 & 0 & 0 \\ 0 & a/b & 0 \\ 0 & 0 & a/c \end{bmatrix} \tag{44}$$

where $a$, $b$, $c$, are the coefficients defining the form of the ellipsoïdal inclusion

$$x^2/a^2 + y^2/b^2 + z^2/c^2 = 1 \tag{45}$$

In the general case of an ellipsoïdal inclusion, the calculation of $\Gamma^{gg}$ results from the numerical integration of (42).

If the matrix is assumed incompressible and isotropic, $A^\circ$ depends on a single parameter $\mu^*$

$$\begin{aligned} A^\circ_{ijkl} &= \mu^*(\delta_{ik}\,\delta_{jl} + \delta_{il}\,\delta_{jk}) \\ &= 2\mu^* I_{ijkl} \end{aligned} \tag{46}$$

Then the Fourier transform of the Green functions are

$$\begin{aligned} \tilde{G}_{ni}(\mathbf{k}) &= \frac{1}{\mu^* k^2}\delta_{ni} - \frac{1}{\mu^* k^4} k_n k_i \\ \tilde{H}_j &= e^{i\pi/2} k_j/k^2 \end{aligned} \tag{47}$$

where $k$ is the norm of the vector $\mathbf{k}$.

If, furthermore, the inclusion is spheroidal, simple analytical expressions are obtained for the $P^{gg}_{ijmn}$

$$\begin{aligned} &P_{1111} = P_{2222} = P_{3333} = -\frac{2}{15\mu^*} \\ &P_{1212} = P_{2121} = P_{1313} = P_{3131} = P_{2323} = P_{3232} = -\frac{4}{15\mu^*} \\ &P_{1122} = P_{2211} = P_{1133} = P_{3311} = P_{2233} = P_{3322} = P_{1221} \\ &\quad = P_{2112} = P_{1331} = P_{3113} = P_{2332} = P_{3223} = \frac{1}{15\mu^*} \end{aligned} \tag{48}$$

All other coefficients are equal to zero.

## References


(1) TAYLOR, G. I. (1938) Plastic strain in metals, *J. Inst. Metals*, **62**, 307.
(2) HONEFF, H. and MECKING, H. (1978) *Textures in Materials* (Edited by G. Gottstein and K. Lücke), Springer, Berlin, p. 265.
(3) IWAKUMA, T. and NEMAT-NASSER, S. (1984) Finite elastic plastic deformation of polycrystalline metals and composites, *Proc. Roy. Soc. Lond.*, *A*, 394, 87.
(4) LIPINSKI, P. and BERVEILLER, M. (1989) Elastoplasticity of micro-homogeneous metals at large strains, *Int. J. Plasticity*, to be published.
(5) NEMAT-NASSER, S. and OBATA, M. (1986) Rate-dependent, finite elasto-plastic deformation of polycrystals, *Proc. Roy. Soc. Lond.*, *A*, 407, 343–375.





(6) MOLINARI, A., CAN large deformation poly
(7) HUTCHINSON, J. W. line materials, *Proc. R*
(8) PAN, J. and RICE, J. surface vertices, *Int. J.*
(9) ASARO, R. J. and NI in rate dependent poly
(10) BERVEILLER, M. a solides hétérogènes, *C* Paris, p. 175.
(11) BACROIX, B. (1986) PhD thesis, McGill Un
(12) LEQUEU, P. H., GI J. J. (1987) Yield surfa *Met.*, 35, 439–451.
(13) HANSEN and LEFFE
(14) TIEM, S., BERVEILI system activity and on

(6) MOLINARI, A., CANOVA, G. R., and AHZI, S. (1987) A self-consistent approach to the large deformation polycrystal viscoplasticity, *Acta Met.*, 35, 2983–2994.
(7) HUTCHINSON, J. W. (1976) Bounds and self-consistent estimates for creep of polycrystalline materials, *Proc. Roy. Soc. Lond., A*, 348, 101–127.
(8) PAN, J. and RICE, J. R. (1983) Rate sensitivity of plastic flow and implications for yield-surface vertices, *Int. J. Solids Structures*, 19, 973–987.
(9) ASARO, R. J. and NEEDLEMAN, A. (1985) Texture development and strain hardening in rate dependent polycrystals, *Acta Met.*, 33, 923–953.
(10) BERVEILLER, M. and ZAOUI, A. (1980) Méthodes self-consistantes en mécanique des solides hétérogènes, *Comptes Rendus du 15° Colloque du Groupe Français de Rhéologie*, Paris, p. 175.
(11) BACROIX, B. (1986) *Prediction of high temperature deformation textures in F.C.C. metals*, PhD thesis, McGill University, Montreal, Canada.
(12) LEQUEU, P. H., GILORMINI, P., MONTHEILLET, F., BACROIX, B., and JONAS, J. J. (1987) Yield surfaces for textured polycrystals, Part 1: crystallographic approach, *Acta Met.*, 35, 439–451.
(13) HANSEN and LEFFERS (1987) Private comunication.
(14) TIEM, S., BERVEILLER, M., and CANOVA, G. R. (1986) Strain shape effects on the slip system activity and on the lattice rotations, *Acta Met.*, 34, 2139.